LAWRENCE
LIVERMORE
NATIONAL
LABORATORY

LLNL-JRNL-588296

# Ringwoodite growth rates from olivine with ~75 ppmw H2O: Metastable olivine must be nearly anhydrous to exist in the mantle transition zone

W. L. Du Frane, T. G. Sharp, J. L. Mosenfelder, K. Leinenweber

October 4, 2012

Physics of Earth Planetary Interiors

## Disclaimer

**Ringwoodite growth rates from olivine with ~75 ppmw $H_2O$: Metastable olivine must be nearly anhydrous to exist in the mantle transition zone**

Wyatt L. Du Frane[a,b,*], Thomas G. Sharp[a], Jed L. Mosenfelder[c], Kurt Leinenweber[a]

[a] *School of Earth and Space Exploration, Arizona State University, Tempe, AZ*

[b] *Atmospheric, Earth and Energy Division, Lawrence Livermore National Laboratory, Livermore, CA*

[c] *Division of Geological and Planetary Sciences, California Institute of Technology, Pasadena, CA*

**Abstract**

It has been previously demonstrated that as little as 300 ppmw $H_2O$ increases wadsleyite and ringwoodite growth rates to magnitudes that are inconsistent with the metastable olivine hypothesis. To further test this hypothesis, we present new ringwoodite growth rate measurements from olivine with ~75 ppmw $H_2O$ at 18 GPa and 700, 900, and 1100 °C. These growth rates are nearly identical to those from olivine with ~300 ppmw $H_2O$, and significantly higher than those from nominally anhydrous olivine. We infer that transformation of olivine with 75-300 ppmw $H_2O$ is primarily enhanced by hydrolytic weakening of reaction rims, which reduces the elastic strain-energy barrier to growth. We present a new method for fitting non-linear nominally anhydrous data, to demonstrate that reduction of growth rates by elastic strain energy is an additional requirement for metastable olivine. Based on previous thermokinetic

modeling, these enhanced growth rates are inconsistent with the persistence of metastable olivine wedges into the mantle transition zone. Metastable persistence of olivine into the mantle transition-zone would therefore require < 75 ppmw $H_2O$.

## 1. Introduction

The metastable olivine hypothesis holds that oceanic lithosphere may be sufficiently cold in some subduction zones to kinetically inhibit the transformation of olivine into its higher-pressure polymorphs, wadsleyite and ringwoodite, in Earth's mantle transition zone (MTZ) (Sung and Burns, 1976a). Metastable olivine is less dense than the surrounding MTZ minerals, so its presence would exert buoyancy-induced forces that could reduce subduction rates (Marton et al., 1999; Tetzlaff and Schmeling, 2000), contribute to slab stagnation (van der Hilst et al., 1991; Tetzlaff and Schmeling, 2009), and change the stress state within the slab by producing a shear stress along the boundaries of a metastable olivine "wedge" (Yoshioka et al., 1997). Rapid transformation of metastable olivine produces anti-cracks that may lead to shear instability, which has been proposed as a trigger mechanism of deep focus earthquakes in the MTZ (e.g. Sung and Burns, 1976b; Burnley and Green, 1989; Green and Burnley, 1989; Burnley et al., 1991; Rubie and Ross, 1994; Kirby et al., 1996). Finally, the existence of metastable olivine in the MTZ would imply limited $H_2O$ contents of host slabs, because transformation kinetics are greatly enhanced by the presence of hydrogen (Kubo et al., 1998a; Hosoya et al., 2005; Diedrich et al., 2009; Kubo et al., 2009; Smyth et al., 2012).

A variety of seismic observations have been attributed to the existence of metastable olivine in some subduction zones. Deep focus earthquake hypocenters (300-700 km depth) occur most frequently in the coldest, oldest slabs with high subduction rates, which suggests a possible link to the presence of metastable olivine (Kirby et al., 1996). Seismic low-velocity zones in the Pacific, Mariana, and Kuril slabs have been interpreted as metastable olivine (Pankow et al., 2002; Kaneshima et al., 2007; Jiang et al., 2008). Seismic anisotropy in the subducting Tonga-Fiji slab and below Northeast Asia has been interpreted as resulting from lattice preferred orientation of metastable olivine (Chen and Brudzinski, 2003; Liu et al., 2008). In addition, double seismic zones in the Tonga, Izu-Bonin, and Pacific slabs have been attributed to delayed, seismogenic transformation at the boundaries of a metastable olivine wedge (Wiens et al., 1993; Iidaka and Furukawa, 1994; Guest et al., 2004). These interpretations of seismic data provide indirect evidence for metastable olivine.

The metastable olivine hypothesis can be tested in the laboratory by measuring transformation kinetics and mechanisms and combining these data with thermo-kinetic models to calculate the depth to which olivine would persist into the MTZ (Rubie and Ross, 1994; Mosenfelder et al., 2001). Olivine transformation rates measured in the laboratory at higher temperature (700-1100 °C) are extrapolated to lower temperatures predicted for the most likely host slabs. The internal temperatures of the oldest and most rapidly subducting slabs, such as those of the Tonga subduction zone, are estimated to be between 500-700 °C at MTZ depths (Kirby et al., 1996), which is approximately 900° cooler than typical MTZ temperatures (Ito and Katsura, 1989). Such reduced temperatures move the olivine-wadsleyite equilibrium phase

boundary to shallower depths within the slab (Akaogi et al., 1989). The lower temperatures would also decrease the olivine transformation rates, and this is the basis of the metastable olivine hypothesis (e.g. Kirby et al., 1996).

Olivine transformation kinetics depend on both nucleation and growth rates. For ringwoodite and wadsleyite, grain-boundary nucleation rates are predicted to be high relative to growth rates under subduction zone conditions (Rubie et al., 1990; Rubie and Ross, 1994). As a result, most ringwoodite and/or wadsleyite growth occurs as a uniform rim in transformation experiments (e.g. Kerschhofer et al., 1996; Kubo et al., 1998a; Diedrich et al., 2009). In this case, transformation is limited by the rim growth rate ($\dot{x}$), which can be determined by measuring rim thickness as a function of time (e.g. Kerschhofer et al., 1996; Kerschhofer et al., 1998; Kerschhofer et al., 2000).

For nominally anhydrous olivine, the wadsleyite and ringwoodite growth rates are time dependent because of the stress associated with volume reduction during the reaction (e.g. Liu et al., 1998). The volume change associated with olivine transformation into wadsleyite (-6%) or ringwoodite (-8%) (Rubie, 1996) results in a volume mismatch between the reaction rim and the olivine core, which remain in contact during transformation. If the rim does not deform fast enough to keep pace with the volume reduction, elastic strain energy builds up and reduces the driving force for rim growth (Kerschhofer et al., 1998; Kubo et al., 1998a; 1998b). The growth rate is therefore limited by the viscoelastic relaxation rate of the growth rim (Liu et al., 1998; Mosenfelder et al., 2000; Morris, 2002). Viscoelastic relaxation rates have not been measured directly, but Mosenfelder et al. (2000) constrained the strength of the wadsleyite growth rims in

samples by modeling the rate of stress relaxation. Buildup of elastic strain could also generate differential stress in the olivine that could enhance heterogeneous intracrystalline nucleation (Liu and Yund, 1995; Kerschhofer et al., 1998). External differential stress on partially transformed olivine may enhance viscoelastic relaxation and deformation of the growth rim, as well as heterogeneous intracrystalline nucleation. The competing mechanisms of rim and intracrystalline growth, in addition to elastic strain energy, complicate transformation kinetics in the case of nominally anhydrous olivine. However, it is essential to also consider how hydrogen affects olivine transformation kinetics and mechanisms because subducting lithosphere may be hydrated to variable extents (Peacock, 2001; Hacker et al., 2003; Ranero et al, 2003).

All previous studies indicate that the presence of hydrogen greatly enhances olivine transformation kinetics (e.g. Kubo et al., 1998a; Hosoya et al., 2005; Diedrich et al., 2009) and thereby reduces the depths to which metastable olivine would persist into the MTZ. Two mechanisms have been suggested for how hydrogen enhances growth rates: 1) Hydrogen may aid diffusion of ions across the growth interface during olivine transformation, by reducing the energy required to break Si-O bonds (Rubie, 1986); 2) Hydrogen may alleviate elastic strain energy by hydrolytically weakening the growth rim (Kubo, 1998; Diedrich et al., 2009), because hydrous ringwoodite is weaker than anhydrous ringwoodite (Inoue et al., 1998; Kavner, 2003). Mosenfelder et al. (2001) also suggested that preferential partitioning of hydrogen into the wadsleyite (e.g. Young et al., 1993) or ringwoodite (e.g., Diedrich et al., 2009) growth rim would reduce hydrogen at the growth interface and in the olivine, decreasing hydrogen-aided diffusion

rates across the growth interface, and making it difficult to separate the respective contributions of these two mechanisms.

Kinetic experiments have been conducted to transform hydrous olivine to wadsleyite and to ringwoodite. Wadsleyite growth rates exhibit a power-law dependence on $H_2O$ contents between 660-5000 ppmw (Hosoya et al., 2005; Kubo et al., 2009). Ringwoodite growth rates from olivine with ~300 ppmw $D_2O$ at 1100 °C and 18 GPa are orders of magnitude faster (with activation enthalpy 237 kJ/mole) (Diedrich, et al., 2009) than for anhydrous olivine (with activation enthalpy of 400 kJ/mole) (Mosenfelder et al., 2001), both of which are higher than those predicted for 300 ppmw $H_2O$ by the Hosoya et al. (2005) model for Wadsleyite. Kubo et al. (1998a) reported that the wadsleyite rim in the sample from their 'dry run' had 200 ppmw $H_2O$, indicating the possibility of $H_2O$ gain during olivine kinetics experiments. No other reported studies on nominally anhydrous or hydrous olivine have tested for $^1H_2O$ gain during transformation runs (Diedrich et al., 2009 only analyzed post run $D_2O$ content).

The quantity of $H_2O$ that is cycled deep into the mantle is not well constrained (Hirschmann et al., 2005), and the strong effect of $H_2O$ on olivine transformation kinetics could provide a means of constraining the $H_2O$ contents of subducting mantle lithosphere; however, better understanding is necessary to make quantitative determinations. Kubo et al. (2009) extrapolated kinetic data measured for olivine with 660-5000 ppmw $H_2O$ by Hosoya et al. (2005) to a lower $H_2O$ content of 150 ppmw to match seismic observations that were inferred to be metastable olivine in the Mariana slab. Recently Green et al. (2010) used experimental data from Diedrich et al. (2009) to conclude that subducting slabs harbor less than 100 ppm $H_2O$.

However, Diedrich et al. did not present data on compositions with < 300 ppm $H_2O$ so the discussion in Green et al. can only pertain to $H_2O$ contents $\geq$ 300 ppm. Here we present ringwoodite growth kinetics for olivine containing as little as 75 ± 15 ppmw $H_2O$. We have thus reduced the $H_2O$ content fourfold, to measure the reaction rates in a new regime that was not explored by Diedrich et al. (2009) and further constrain the maximum allowable $H_2O$ content of subducting slabs containing metastable olivine. This represents the first actual data in this regime, and can bring the discussion of low $H_2O$ contents beyond inference and into the realm of measurement.

## 2. Experimental Techniques

### *2.1 Olivine hydration*

Our transformation experiments were performed in a two-step process similar to that of Diedrich et al. (2009), with olivine first hydrated at 2 GPa, and then transformed at 18 GPa. Single crystals of San Carlos (AZ) olivine were ground into spheres in a bond-type mill (Nitkiewicz and Sterner, 1988) in order to simplify rim growth analysis. The spheres were sieved to 425-500 µm diameter. The spheres were then hydrated at 2 GPa and 950 ˚C for 48 hours, using the capsule design of Diedrich et al. (2009) modified for use in a ½" non-end loaded piston-cylinder apparatus (Table 1). San Carlos enstatite grains were included to buffer the silica activity during hydration. Distilled deionized water was injected into the capsule, which provided a hydrostatic fluid pressure medium that prevented grain impingement. The sample and fluid were contained in a thick-walled (1 mm) Ag capsule. Au foil (0.127 mm thick) lined the inside

of the Ag capsule and lid to prevent sample Fe loss, and to seal the capsule to the lid during pressurization. Pyrophyllite outer capsules (2 lids and a sleeve) were used to retard $H_2O$ loss (Freda et al., 2001) and insulate the inner Ag capsule from the graphite furnace. A Ni foil disk was placed in the bottom of the capsule and separated from olivine by $Ag_{70}Pd_{30}$ foil, to maintain oxygen fugacity at the Ni-NiO buffer. A visible nickel-bearing olivine (NiO/(NiO+MgO+FeO) = 5-10 % measured by electron microprobe) layer ($\leq$ 50 μm) precipitated unevenly on some spheres in the PC22 run, but these spheres were not used in transformation experiments.

*2.2. Transformation*

Experimentally hydrated olivine spheres were partially transformed in the multi-anvil press at 18 GPa and 700, 900, and 1100 $^{\circ}$C, for durations ranging between 2 minutes and 96 hours. We used the COMPRES 10:5 assembly developed and calibrated by T. Diedrich and K. Leinenweber (Diedrich et al., 2009; Leinenweber et al. 2012). As a control, we also transformed nominally anhydrous samples at 18 GPa and 1000 $^{\circ}$C. Silver capsules were used to reduce hydrogen loss or gain during the experiment. Two spheres were used for each experiment, with Ag shavings to separate the spheres and fill remaining space in the capsule. A silver lid was cold-sealed onto the capsule during pressurization. Samples were compressed to 18 GPa over ~10 to 11 hours, and then heated to the target temperature in < 5 minutes. Further experimental details are provided in Diedrich et al. (2009).

Our initial transformation runs were prone to small $H_2O$ gains (~30 ppmw on average, ranging between ~0-80 ppmw; Tables 2 and 3), which were associated with our source and

preparation of Ag capsules (hereafter referred to as 'method 1'). We subsequently modified our experimental procedure to exactly match that of T. Diedrich (pers. comm.). This procedure (hereafter referred to as 'method 2') included: 1) eliminating use of oil for machining of capsules, and 2) annealing capsules prior to assembly (800 °C for 1 hour) to remove surface contaminants. This also reversed the effects of work hardening, allowing the capsules to seal more efficiently. Method 2 reduced $H_2O$ gains to < 10 ppmw during transformation (Table 2 and 3). One exception, BB688, was a particularly long experiment (30 hrs at 1000 °C) that likely gained $H_2O$ via diffusion through the Ag capsule.

*2.3. $H_2O$ Measurement*

The $H_2O$ contents of hydrated starting spheres and transformed samples were measured using Fourier transform infrared (FTIR) spectroscopy and secondary ion mass spectrometry (SIMS). FTIR and SIMS measurements on a Cameca 7f-GEO were performed at the California Institute of Technology (see Mosenfelder et al. 2011 for details). SIMS measurements on a Cameca 6f were performed at Arizona State University.

For SIMS measurements, samples were polished, cleaned, and mounted in indium following the procedure of Aubaud et al. (2007). The instruments were baked out at high vacuum to minimize hydrogen background (Aubaud et al., 2007). To analyze hydrogen we counted $^{16}O^{1}H$ secondary species normalized to $^{30}Si$ counts, using a 5-10 nA $Cs^+$ primary beam with 20 keV impact energy, 20 μm raster, and mass resolving power of $M/\Delta M = 5000$. Measurements on the Cameca 7f-GEO were calibrated using natural olivine standards (characterized by FTIR;

Mosenfelder et al. 2011) present on each sample mount. Measurements on the Cameca 6f were performed standard-less, directly following instrument calibration by Tenner et al. (2009), and applying the corrected olivine calibration in Withers et al. (2011).

For FTIR measurements of hydrated olivine spheres, we measured the total absorbance in two doubly polished planes of olivine with **E** parallel to the [100], [010], and [001] orientations over the spectral range 3100-3750 $cm^{-1}$. The total integrated absorbance over this range for all three principal orientations of olivine is proportional to bulk $H_2O$ content (Bell et al., 2003). We also measured some partially transformed samples using a 25 μm x 25 μm aperture with **E** approximately parallel to [100] (the principal orientation with the highest absorbance); this measurement allowed us to estimate $H_2O$ contents and distribution in the unreacted olivine and the cores of reacted olivine samples. The crystallographic orientation was estimated in partially transformed olivine from silicate overtone bands (Asimow et al., 2006).

## 3. Results

### *3.1 $H_2O$ contents of hydrated olivine spheres*

FTIR spectra were collected on one of the spheres from the PC22 hydrating run in the piston cylinder. Total absorbance was measured with **E** parallel to the [100], [010] and [001] orientations in these samples (Fig. 1), resulting in a concentrations measurement of 88 ±9. SIMS was performed on hydrated spheres from 6 different runs. Measurements on the Cameca 7f, calibrated by standards on the sample mount, resulted in an average concentration of 68ppmw $H_2O$. Measurements on the Cameca 6f using the previous calibration by Tenner et al. (2009) and

Withers et al. (2011) resulted in an average concentration of 60 ppmw $H_2O$, which is in good agreement with other measurements performed using FTIR and the Cameca 7f (Table 1). These measurements demonstrate that our hydration experiments consistently produced olivine spheres with reproducible, homogenous $H_2O$ contents of ~75 ppmw.

*3.2 Growth Rim Analysis*

Most of the growth in our partially transformed samples occurred in uniform rims (Fig. 2), indicating that surface nucleation sites were saturated. We only report rim growth rates here, although relatively small amounts of intracrystalline growth also occurred in the olivine cores of our samples. Partially transformed spheres were cut with a diamond embedded wire-saw and doubly polished into thin sections (< 50 μm) for petrographic analysis. We sectioned the center of reacted olivine spheres by carefully polishing from two sides and paying attention to how much material was removed from each side, so that the observed rim thickness was equal to the true rim thickness. We measured the average radii of the olivine cores and growth rims in each thin section to determine rim thickness. Errors we report are estimated as one standard deviation of ~50 linear measurements of thickness throughout the growth rim in each thin section (Tables 2 and 3; Fig. 2). Growth rim thickness data (x) are fit to a linear function of run duration (t),

$$\dot{x} = \Delta x/\Delta t \quad (1)$$

where the slope of the line is $\dot{x}$, the average growth rate (e.g. Diedrich et al., 2009). Growth rates can be expressed as a function of temperature and pressure using the following equations,

$$\dot{x} = (k_0 T)(e^{-\frac{\Delta H_a}{RT}})(1 - e^{\frac{\Delta G_{rxn}}{RT}}) \quad (2a)$$

$$\Delta H_a = \Delta E_a + P\Delta V_a \quad (2b)$$

where $k_0$ is a pre-exponential factor, T is absolute temperature, $\Delta H_a$ is activation enthalpy, $\Delta G_{rxn}$ is the Gibbs free energy change, P is pressure, $\Delta V_a$ is activation volume, and $\Delta E_a$ is activation energy (Turnbull, 1956). We calculated $\Delta G_{rxn}$ from data by Akaogi et al. (1989). Activation volume could not be determined from our isobaric experiments; therefore, we used published estimates of $\Delta V_a = 0$ $cm^3$/mole (Burnley, 1995) and $\Delta V_a = 3.3$ $cm^3$/mole (Hosoya et al., 2005) to calculate activation energy.

Raman spectra were measured throughout the reaction rims and cores of 4 of the samples (BB527, BB616, BB653, BB656). Phases were identified by comparing spectra with those in the RRUFF online database (rruff.info/). Optical analyses and Raman spectroscopy of the samples indicate that the growth rims are ringwoodite, and that the cores remained as olivine. Wadsleyite was not detected in the Raman spectra that were collected on our samples, but previous studies have shown that the reaction rims on nominally anhydrous olivine, transformed in the ringwoodite stability field, generally contain both ringwoodite and wadsleyite (Kerschhofer et al, 1998, Diedrich et al. 2009).

*3.3 $H_2O$ contents of partially transformed samples*

$H_2O$ contents and distributions were measured in the olivine cores of partially transformed samples by both SIMS and FTIR and were in good agreement (Tables 2 and 3). For example, both techniques indicate that there is 12-14 ppmw $H_2O$ in the center of the olivine core for sample BB622 (Fig. 3). Some SIMS spot analyses of olivine indicated higher $H_2O$ contents

than in nearby or surrounding regions; this may be due to inclusion of intracrystalline ringwoodite or wadsleyite. FTIR spectra of the olivine cores of some samples exhibited O-H absorption coefficients resembling those of ringwoodite, and in one sample (BB680) wadsleyite.

Quantitative measurements of $H_2O$ in growth rims were not possible due to the technical difficulties of isolating them from olivine cores and contamination by surface $H_2O$ and/or organic material introduced during sample preparation. For FTIR measurements, sufficient sample thickness and aperture areas were required to obtain suitable spectra, and this did not allow us to entirely isolate growth rims from neighboring olivine and silver. Therefore, we were only able to estimate minimum $H_2O$ contents in some sufficiently thick polycrystalline growth rims using unpolarized FTIR with calibration from Paterson (1982). SIMS measurements performed on polycrystalline growth rims suffered from the prevalence of grain boundaries, cracks and pits that hosted variable amounts of contaminant hydrogen. This problem was apparent from very large discrepancies in both $^{16}O$-$^{1}H$ and $^{12}C$ measurements made adjacently within the same sample rims, which indicates that the measurements include variable amounts of hydrocarbon materials gained during polishing. For these reasons, we were only able to estimate maximum $H_2O$ contents in some growth rims using SIMS (Tables 2 and 3).

An approximation of the ratio of $H_2O$ in the olivine core to the growth rim can be combined with measurements of $H_2O$ contents in olivine cores, average radii for the core and rim in thin section, and assumed spherical geometry to estimate the final bulk $H_2O$ contents of our samples (Table 2 and 3). The average ratio of $H_2O$ measured in the olivine core to the maximum $H_2O$ estimated in the growth rim is 12.8, which would imply that ‘method 1’ were prone to

variable gains up to ~330 ppmw $H_2O$, and those transformed by 'method 2' gained $\leq$ ~11 ppmw $H_2O$ (except BB688). However, all of our SIMS measurements of the growth rim were affected by variable amounts of additional $H_2O$ from materials gained in cracks and pits during polishing of our samples. These polishing materials are unlikely to contain any significant $D_2O$ that would affect SIMS measurements of $D_2O$ contents. Therefore, $D_2O$ measurements provide a more accurate approximation of the ratio of $H_2O$ in ringwoodite to olivine for our partially transformed samples. A sample at partially transformed 900 °C and 18 GPa (Diedrich et al., 2009) has a measured ratio of 3.4 $D_2O$ in ringwoodite to olivine. Using this ratio instead, we estimate that samples transformed by method 1 were prone to small variable gains of up to ~80 ppmw $H_2O$, and those transformed by method 2 gained $\leq$ ~6 ppmw $H_2O$ (Table 2 and 3, except BB688). For sample BB688 (method 2) we measured an average of 18 ppmw in the olivine core and estimate ~200-300 ppmw $H_2O$ in the rim; however, this sample was transformed for 30 hrs at 1000 °C, which may have been too long to prevent $H_2O$ gained from outside the sample via diffusion through the Ag capsule.

*3.4. Growth rates for nominally anhydrous olivine*

Transformation experiments were performed on nominally anhydrous olivine spheres (only using method 2, with < 10 ppmw $H_2O$ gain) at 18 GPa and 1000 °C. Rim growth rates were non-linear, and decreased with increased run duration (Fig. 4). Previous studies have treated growth rates measured from nominally anhydrous olivine as being initially linear (e.g. Liu et al., 1998; Mosenfelder et al., 2001; Diedrich et al., 2009). By comparing the measured rim

thicknesses of experiments at 1000 °C with different durations we use Equation 1 to estimate average growth rates of 5.9 x $10^{-9}$ m/s between 0-10 minutes, 3.7 x $10^{-9}$ m/s between 10-26 minutes, 1.8 x $10^{-9}$ m/s between 26-60 minutes, and 6.8 x $10^{-11}$ m/s between 60-360 minutes (Fig. 4A). These data imply that the growth rates likely decreased exponentially with time from the onset of growth, rather than growing at an initially constant rate. Fitting decreasing growth rates as a function of time allows us to calculate the initial growth rate (t = 0) and provides a better method for comparison of data collected from different conditions or studies (Fig. 4B). We calculate that the initial growth rate for nominally anhydrous olivine is 5.2 x $10^{-9}$ m/s at 1000 °C using data from this study. We also calculate that the initial growth rate for nominally anhydrous olivine is 7.1 x $10^{-9}$ m/s at 1100 °C using data from Diedrich et al. (2009), which is higher than the growth rate fit of 4.0 x $10^{-9}$ m/s that assumes constant rate for the first 60 minutes of growth. We excluded experiments that were at T $\geq$ 1000 °C for $\geq$ 24 hours from these fits due to the likelihood of $H_2O$ diffusion through the Ag capsule, as was verified to be the case in experiment BB688 (Table 2).

*3.5. Growth rates for hydrated olivine*

Olivine containing ~75 ppmw $H_2O$ was transformed at 18 GPa, between 700-1100 °C. All rim growth rates measured from hydrous olivine spheres were higher than those measured from nominally anhydrous olivine. Raman spectra and optical analysis of thin sections indicate that growth rims were ringwoodite and cores were olivine. At 700 and 900 °C, growth-rim thicknesses had a nearly linear relationship with run duration (Figs. 2, 5A, and 5B). This contrasts with the growth rates measured for nominally anhydrous olivine that continually

decreased during transformation. By fitting rim thickness data (weighted by error) to equation 1 we obtain ringwoodite growth rates of 2.9 (± 1.4) x $10^{-11}$ m/s at 700 °C and 1.4 (± 0.2) x $10^{-9}$ m/s 900 °C. At 1100 °C, ringwoodite grew faster from hydrous olivine than nominally anhydrous olivine, but decreased with time. The first ~40 μms of the rim grew relatively rapidly in 5-10 minutes until ~50% of the overall volume of the olivine sphere with ~500 μm radius had transformed (Fig. 5C). A weighted fit of the first 2 experiments (2 and 5 minutes) provides an initial growth rate of 1.0 (± 0.3) x $10^{-7}$ m/s at 1100 °C (Fig. 6). The rim thickness values for runs $\geq$ 10 min are not significantly greater than 40 μm, indicating that the growth rate dropped drastically after ~50% of the sample had transformed (Fig. 5C). Growth rate measurements decreased with duration at these conditions (1100 °C, 18 GPa) because they are closer to equilibrium, which results in a lower $\Delta G_{rxn}$ value.

Growth rates at 700, 900 °C, and the initial rate at 1100 °C (Fig. 6) were fit to equation 2b (weighted by error) to obtain $\Delta H_a$ = 227 +/- 32 kJ/mol at 18 GPa, $\Delta E_a$ = 227 +/- 32 kJ/mol for $\Delta V_a$ = 0 $cm^3$/mole, and $\Delta E_a$ = 178 +/- 32 kJ/mol for $\Delta V_a$ = 3.3 $cm^3$/mole. Several other fitting methods were also examined, with the results summarized in Table 4: fitting without weighting by error; fits allowing rim thickness at t = 0 to vary; and separate fits obtained using experimental methods 1 or 2. These variations had small effects on resulting growth rate and activation enthalpy values.

**4. Discussion**

The ringwoodite-rim growth rates at 18 GPa and 700 and 900 °C for olivine with 75 ppmw $H_2O$ are similar to those of olivine with 300 ppmw $D_2O$ (Diedrich et al., 2009). The rim thickness data from these two studies overlap within error (Fig. 4A and 4B). Rim thicknesses grew at nearly linear rates at 900 °C, where the longest experiment (26 hours) suggests only a slight decrease in growth rate (Figs. 5B). This result is similar to the slight downward curvature of rim thickness data for olivine with 300 ppmw $D_2O$ at 900 and 1100 °C (Diedrich et al., 2009). The ringwoodite-rim growth rates for olivine with ~75 ppmw $H_2O$ at 18 GPa and 1100 °C were not constant over the durations examined in this study. The initial growth rate we fit from 2 and 5 minute runs using olivine with ~75 ppmw $H_2O$ was similar in magnitude to the nearly constant, overall growth rate measured in olivine with ~300 ppmw $D_2O$ over (Diedrich et al., 2009). However, for olivine with ~75 ppmw $H_2O$, the growth rate decreased substantially after the rim grew to ~40 μm thick in 5 minutes (Fig. 5C). We can estimate $H_2O$ concentration of the growth rim using measurements of the olivine core with the approximate partition coefficient of 3.4 for $D_2O$ in ringwoodite to olivine (Diedrich et al., 2009). Ringwoodite rims with 400-600 ppmw $D_2O$ (Fig. 9 and 12 in Diedrich et al., 2009) do not show the significant decrease in the growth rate, but those with 140-240 ppmw (=3.4 x 42 to 3.4 x 72 ppmw $H_2O$ in Run BB550 and 588) exhibit substantial decrease in growth rate with time (Fig. 6). Therefore the threshold amount of hydrogen necessary to sufficiently weaken the ringwoodite growth rim is likely in between these values. This compares favorably with previous measurements of growth rates for Fe-bearing wadsleyite with 200-500 ppmw $H_2O$ that decreased with time at temperatures $\geq$ 1030 °C (Kubo et al., 1998a; 1998b).

The Hosoya et al. (2005) model predicts growth rates for olivine with 75 ppmw $H_2O$ and 300 ppmw $H_2O$ that are significantly lower than those measured in this study and in Diedrich et al. (2009) (Fig. 6). Experimental differences may account for some of these discrepancies. Elastic strain energy associated with olivine-wadsleyite transformation (-6% volume change) is less than for olivine-ringwoodite transformation (-8% volume change). The olivine grain sizes (425-500 μm) and Fe content ($Fo_{91}$) of samples in this study better resemble those observed in mantle xenoliths (e.g. Frey and Prinz, 1978; Armienti and Tarquin, 2002) than samples studied by Hosoya et al. (2005) ($Fo_{100}$, 5-7 μm). The effects of elastic strain energy are likely to be less for smaller grain sizes due to higher surface area to volume ratio. Additionally the elastic strain energy effects may be influenced somewhat by the different experimental assemblies used. The role of Fe on olivine transformation has not been studied, but Fe content affects the mechanisms for hydrogen incorporation (Mosenfelder et al., 2006; Zhao et al., 2004).

The similarity in ringwoodite growth rates measured in olivine with either 75 ppmw $H_2O$ or 300 ppmw $D_2O$ suggests that the rates do not depend strongly on $H_2O$ contents between 75-300 ppmw (assuming that hydrogen and deuterium have the same or similar effects). If true, the observed power-law dependence of wadsleyite growth rates on $H_2O$ contents $\geq$ 660 ppmw (Hosoya et al., 2005) may not extrapolate accurately to $H_2O$ contents $<$ 300 ppmw. The mechanism of hydrogen-aided diffusion is likely to be sensitive to $H_2O$ content, and may therefore be the dominant mechanism of growth rate enhancement for $\geq$ 660 ppmw $H_2O$ (Hosoya et al., 2005). Alternatively, a hydrolytic weakening mechanism would be insensitive to $H_2O$ contents, if there is a threshold $H_2O$ concentration that sufficiently weakens ringwoodite rims to

allow growth-rim deformation to keep pace with the volume change associated with transformation. The exact mechanism of hydrolytic weakening and its dependence on $H_2O$ contents are not well constrained for ringwoodite, but in this case the growth rim only needs to be weakened enough to prevent buildup of significant stress at the growth interface. Therefore, the hydrolytic weakening mechanism better explains ringwoodite-rim growth rates that are significantly higher than nominally anhydrous olivine, but insensitive to $H_2O$ concentration in 75-300 ppmw range.

We propose that during olivine transformation, hydrogen partitions into growth rims, allowing them to deform. Rim deformation can proceed as long as the $H_2O$ concentration of the rim remains above a threshold level. The amount of $H_2O$ between 75-300 ppmw does not seem to alter the initial growth rate, but instead determines how long the growth rate will remain high, constant, and unimpeded by the build-up of elastic strain energy. Based on our experiments at 18 GPa and 900 °C, a bulk hydrogen content of 75 ppmw $H_2O$ seems to satisfy this requirement for nearly complete transformation. Our experiments at 18 GPa, 1100 °C were closer to the olivine-ringwoodite phase boundary, which likely explains why these measurements were more strongly affected by elastic strain energy. The ringwoodite growth rims appear to become stronger as the volume fraction increases and their bulk $H_2O$ concentration decreases. With decreasing hydrolytic weakening of the growth rim, the elastic strain energy would build up, causing ringwoodite growth rates to decrease (e.g. Liu et al., 1998).

Extrapolation of laboratory measurements to temperatures relevant to the coldest subduction zones (500-700 °C, Kirby et al., 1996) results in ringwoodite growth rates for olivine

with 75 ppmw $H_2O$ and 300 ppmw $D_2O$ that are many orders of magnitude higher than those used in previous thermokinetic models (Mosenfelder et al., 2001 using "nominally dry" olivine; Kubo et al., 2009 using olivine with 150 ppmw $H_2O$) (Fig. 6). Thermokinetic modeling was performed using the model developed and published in Mosenfelder et al. (2001) with growth rate and activation enthalpy data from Diedrich et al. (2005; 2009) to verify that growth rates of these magnitude are incompatible with a metastable wedge in any subducting slab (Marton et al., 2006). These growth rates imply that a metastable wedge of olivine in a subduction zone, as inferred from geophysical studies, requires the subducting mantle lithosphere to have less than 75 ppmw $H_2O$. Consequentially, the existence of metastable olivine imposes constraints on the overall amount of $H_2O$ that would be cycled to the MTZ via subduction.

Previous studies on nominally anhydrous olivine have attempted to resolve linear, initial growth rates unaffected by the buildup of elastic strain energy by fitting only the shortest duration data (e.g. Liu et al., 1998; Mosenfelder et al., 2001; Diedrich et al., 2009). The average rim growth rate we derive for nominally anhydrous olivine after 10 minutes at 18 GPa and 1000 °C, is only a factor of 2-3 smaller than the growth rate fit we obtain for hydrous olivine (Fig. 4A). For nominally anhydrous olivine at 18GPa and, fitting data up to six hours yielded an initial (t = 0) ringwoodite rim growth rates of $5.2 \times 10^{-9}$ m/s at 1000 °C and $7.1 \times 10^{-9}$ m/s at 1100 °C. These initial growth rates are only slightly less than those we measured for olivine with 75 ppmw $H_2O$, but they decreased with duration at an average rate of ~2% per minute (Fig. 4B). If elastic strain energy accumulates at the onset of growth, then the previously used fitting method would slightly underestimate initial growth rates for nominally anhydrous olivine (Fig. 6). These errors

become magnified by extrapolation to 500-700 °C. This makes it essential to consider to what extent these elastic strain effects inhibit olivine transformation in the Earth. If viscoelastic relaxation of wadsleyite or ringwoodite growth rims occurs at rates that are high enough to eliminate elastic strain energy effects over the timescales and conditions of a subduction zone, then growth rates from nominally anhydrous olivine in the MTZ could be constant and remain similar in magnitude to the initial growth rates we calculated for t = 0 (Fig. 6). In this case, elastic strain energy buildup at the growth interface would be a requirement for metastable olivine regardless of whether or not $H_2O$ is present. Additionally, intracrystalline transformation may contribute significantly to reducing the extent of olivine metastability at 18 GPa. Future thermokinetic models should consider the effects of elastic strain energy on olivine transformation kinetics and the contributions of intracrystalline growth to fully test the metastable olivine hypothesis.

## 5. Conclusions

Small amounts of $H_2O$ have a substantial effect on olivine transformation kinetics. Olivine containing ~75 ppmw $H_2O$ transforms at a higher, initially constant rate in comparison to continually decreasing rate for nominally anhydrous olivine. At 900 °C and 18 GPa, ~75 ppmw $H_2O$ allowed for transformation of most of the olivine samples at an enhanced rate. However, 75 ppmw $H_2O$ was not enough to complete transformation of the olivine at an enhanced rate at 1100 °C and 18 GPa due to the close proximity of these conditions to the phase equilibrium boundary and lower $\Delta G_{rxn}$ value. We interpret the enhancement of transformation and growth rates by 75-

300 ppmw $H_2O$ in the olivine starting material to be the result of hydrolytic weakening of the growth rim, reducing elastic strain energy and its effects.

Our results combined with previous thermokinetic modeling indicate that olivine must contain < 75 ppmw $H_2O$ for a metastable wedge to persist into the MTZ in even the most likely subducting slabs, such as Tonga. Therefore, the existence of metastable olivine would have ramifications for the entire deep earth $H_2O$ cycle. Previous thermokinetic models are based on the assumption that growth rates are constant and unaffected by elastic strain energy at growth interfaces. This assumption may be appropriate for olivine containing > 75 ppmw $H_2O$, but may not be correct for olivine containing < 75 ppmw $H_2O$. If our interpretation that hydrogen increases growth rates by hydrolytic weakening of the growth rim is correct, than elastic strain energy buildup at growth interfaces is an additional requirement for metastable olivine to persist into the MTZ.

**Acknowledgements**

We thank T. Diedrich and G. Moore for help with experiments conducted at the ASU OmniPressure lab; K. Roggensack for assistance with sample sectioning; E. Soignard and R. Tricky for assistance with Raman; and T. Tenner, A. Withers, and M. Hirschmann for providing their assistance with SIMS calibration and measurements on the Cameca 6f at ASU. We thank T. Kubo and D. Rubie for their reviews and comments that helped us significantly improve this manuscript. SIMS data were obtained at the ASU National SIMS Facility, supported by NSF EAR-0622775 to R. Hervig and P.Williams. SIMS data obtained at the Center for Microanalysis

at Caltech were partially supported by the Gordon and Betty Moore Foundation. We acknowledge the LeRoy-Eyring Center for Solid State Science for access to Raman and SEM instrumentation. This work was supported by NSF EAR- 0838159 to T. Sharp and NSF EAR-0947956 to G. Rossman. This work performed under the auspices of the U.S. Department of Energy by Lawrence Livermore National Laboratory under Contract DE-AC52-07NA27344.

**References**

Akaogi, M., Ito, E. and Navrotsky, A., 1989. Olivine-modified spinel-spinel transitions in the system $Mg_2SiO_4$-$Fe_2SiO_4$ - calorimetric measurements, Thermochemical Calculation, and Geophysical Application. J. Geophys. Res - Solid Earth Planets, 94(B11): 15671-15685.

Armienti, P. and Tarquini, S., 2002. Power law olivine crystal size distributions in lithospheric mantle xenoliths. Lithos, 65(3-4): 273-285.

Asimow, P.D., Stein, L.C., Mosenfelder, J.L. and Rossman, G.R., 2006. Quantitative polarized infrared analysis of trace OH in populations of randomly oriented mineral grains. Amer. Mineral., 91(2-3): 278-284.

Aubaud, C., Withers, A.C., Hirschmann, M.M., Guan, Y.B., Leshin, L.A., Mackwell, S.J., and Bell, D.R., 2007. Intercalibration of FTIR and SIMS for hydrogen measurements in glasses and nominally anhydrous minerals. Amer. Mineral., 92(5-6): 811-828.

Bell, D.R., Rossman, G.R., Maldener, J., Endisch, D. and Rauch, F., 2003. Hydroxide in olivine: A quantitative determination of the absolute amount and calibration of the IR spectrum. J. Geophys. Res. - Solid Earth, 108(B2).

Burnley, P.C., 1995. The fate of olivine in subducting slabs: a reconnaissance study. Amer. Mineral., 80(11‐12): 1293‐1301.

Burnley, P.C. and Green, H.W., 1989. Stress dependence of the mechanism of the olivine spinel transformation. Nature, 338(6218): 753-756.

Burnley, P.C., Green, H.W. and Prior, D.J., 1991. Faulting associated with the olivine to spinel transformation in $Mg_2GeO_4$ and its implications for deep-focus earthquakes. J. Geophys. Res. - Solid Earth Planets, 96(B1): 425-443.

Chen, W.P. and Brudzinski, M.R., 2003. Seismic anisotropy in the mantle transition zone beneath Fiji-Tonga. Geophys. Res. Lett., 30(13): 4.

Diedrich, T., Sharp, T.G., and Leinenweber, K., 2005. Experimental study of the effect of water on olivine-ringwoodite transformation rate. Eos Trans. AGU, 86(52), Fall Meet. Suppl., Abstract V41A-1434.

Diedrich, T., Sharp, T.G., Leinenweber, K. and Holloway, J.R., 2009. The effect of small amounts of H2O on olivine to ringwoodite transformation growth rates and implications for subduction of metastable olivine. Chem. Geol., 262(1-2): 87-99.

Freda, C., Baker, D. R., and Ottoloni, L., 2001. Reduction of water loss from gold-palladium capsules during piston cylinder experiments by use of pyrophyllite powder. Amer. Mineral., 86(3): 234-237.

Frey, F.A. and Prinz, M., 1978. Ultramafic inclusions from San-Carlos, Arizona - petrologic and geochemical data bearing on their petrogenesis. Earth Planet. Sci. Lett., 38(1): 129-176.

Green, H.W. and Burnley, P.C., 1989. A new self-organizing mechanism for deep-focus earthquakes, Nature, 341(6244), 733-737.

Green, H.W., Chen, W.P., Brudzinski, M.R., 2010. Seismic evidence of negligible water carried below 400-km depth in subducting lithosphere, Nature, 467(7317): 828-831.

Guest, A., Schubert, G. and Gable, C.W., 2004. Stresses along the metastable wedge of olivine in a subducting slab: possible explanation for the Tonga double seismic layer. Phys. Earth Planet. Inter., 141(4): 253-267.

Hacker, B.R., Peacock, S.M., Abers, G.A., and Holloway, S.D., 2003. Subduction factory: 2. Are intermediate-depth earthquakes in subducting slabs linked to metamorphic dehydration reactions? J. Geophys. Res., 108(B1): 2030.

Hirschmann, M.M., Aubaud, C. and Withers, A.C., 2005. Storage capacity of $H_2O$ in nominally anhydrous minerals in the upper mantle. Earth Planet. Sci. Lett., 236(1-2): 167-181.

Hosoya, T., Kubo, T., Ohtani, E., Sano, A. and Funakoshi, K., 2005. Water controls the fields of metastable olivine in cold subducting slabs. Geophys. Res. Lett., 32(17).

Iidaka, T. and Furukawa, Y., 1994. Double seismic zone for deep earthquakes in the Izu-Bonin subduction zone. Science, 263(5150): 1116-1118.

Inoue, T., Weidner, D.J., Northrup, P.A. and Parise, J.B., 1998. Elastic properties of hydrous ringwoodite (gamma-phase) in $Mg_2SiO_4$. Earth Planet. Sci. Lett., 160(1-2): 107-113.

Ito, E., and Katsura, T., 1989. A temperature profile of the mantle transition zone. Geophys. Res. Lett., 16(5), 425-428.

Jiang, G.M., Zhao, D.P. and Zhang, G.B., 2008. Seismic evidence for a metastable olivine wedge in the subducting Pacific slab under Japan Sea. Earth Planet. Sci. Lett., 270(3-4): 300-307.

Kaneshima, S., Okamoto, T. and Takenaka, H., 2007. Evidence for a metastable olivine wedge inside the subducted Mariana slab. Earth Planet. Sci. Lett., 258(1-2): 219-227.

Kavner, A., 2003. Elasticity and strength of hydrous ringwoodite at high pressure. Earth Planet. Sci. Lett., 214(3-4): 645-654.

Kerschhofer, L., Dupas, C., Liu, M., Sharp, T.G. Durham W.B., Rubie, D.C., 1998. Polymorphic transformations between olivine, wadsleyite and ringwoodite: mechanisms of intracrystalline nucleation and the role of elastic strain. Mineral. Mag., 62(5): 617-638.

Kerschhofer, L., Rubie, D.C., Sharp, T.G., McConnell, J.D.C. and Dupas-Bruzek, C., 2000. Kinetics of intracrystalline olivine-ringwoodite transformation. Phys. Earth Planet. Inter., 121(1-2): 59-76.

Kerschhofer, L., Sharp, T.G. and Rubie, D.C., 1996. Intracrystalline transformation of olivine to wadsleyite and ringwoodite under subduction zone conditions. Science, 274(5284): 79-81.

Kirby, S.H., Stein, S., Okal, E.A. and Rubie, D.C., 1996. Metastable mantle phase transformations and deep earthquakes in subducting oceanic lithosphere. Rev. Geophys., 34(2): 261-306.

Kubo, T., Kaneshima, S., Torii, Y. and Yoshioka, S., 2009. Seismological and experimental constraints on metastable phase transformations and rheology of the Mariana slab. Earth Planet. Sci. Lett., 287(1-2): 12-23.

Kubo, T., Ohtani, E., Kato, T., Shinmei, T. and Fujino, K., 1998a. Effects of water on the alpha-beta transformation kinetics in San Carlos Olivine. Science, 281(5373): 85-87.

Kubo, T., Ohtani, E., Kato, T., Shinmei, T., Fujino, K., 1998b. Experimental investigation of the alpha-beta transformation of San Carlos olivine single crystal. Phys.

Chem. Miner. 26 (1): 1‑6.

Leinenweber, K.D., Tyburczy, J.A., Sharp, T.G., Diedrich, T., Petuskey, W.B., Wang, Y. and Mosenfelder, J.A., 2012. Cell assemblies for reproducible multi-anvil experiments (the COMPRES assemblies). Am. Mineral., 97(2-3): 353–368.

Liu, K.H., Gao, S.S., Gao, Y. and Wu, J., 2008. Shear wave splitting and mantle flow associated with the deflected Pacific slab beneath northeast Asia. J. Geophys. Res. - Solid Earth, 113(B1): 15.

Liu, M., Kerschhofer, L., Mosenfelder, J.L. and Rubie, D.C., 1998. The effect of strain energy on growth rates during the olivine-spinel transformation and implications for olivine metastability in subducting slabs. J. Geophys. Res. - Solid Earth, 103(B10): 23897-23909.

Liu, M. and Yund, R.A., 1995. The elastic strain-energy associated with the olivine-spinel transformation and its implications. Phys. Earth Planet. Inter., 89(3-4): 177-197.

Marton, F.C., Bina, C.R., Stein, S. and Rubie, D.C., 1999. Effects of slab mineralogy on subduction rates. Geophys. Res. Lett., 26(1): 119-122.

Marton, F.C., Diedrich, T., and Sharp, T.G., 2006. Effect of water on olivine metastability in subducting lithosphere. Eos Trans. AGU, Fall Meet. Suppl., Abstract MR11A-0106.

Morris, S., 2002. Coupling of interface kinetics and transformation-induced strain during pressure-induced solid-solid phase changes. J. Mech. Phys. Solids, 50: 1363-1395.

Mosenfelder, J.L., Connolly, J.A.D., Rubie, D.C. and Liu, M., 2000. Strength of $(Mg,Fe)_2SiO_4$ wadsleyite determined by relaxation of transformation stress. Phys. Earth Planet. Inter., 120(1-2): 63-78.

Mosenfelder, J.L., Deligne, N.I., Asimow, P.D. and Rossman, G.R., 2006. Hydrogen incorporation in olivine from 2-12 GPa. Amer. Mineral., 91(2-3): 285-294.

Mosenfelder, J.L., Le Voyer, M., Rossman, G.R., Guan, Y., Bell, D.R., Asimow, P.D. and Eiler, J.M., 2011. Analysis of hydrogen in olivine by SIMS: evaluation of standards and protocol. Amer. Mineral., 96, 1725-1741.

Mosenfelder, J.L., Marton, F.C., Ross, C.R., Kerschhofer, L. and Rubie, D.C., 2001. Experimental constraints on the depth of olivine metastability in subducting lithosphere. Phys. Earth Planet. Inter., 127(1-4): 165-180.

Nitkiewicz, A.M. and Sterner, S.M., 1988. An improved bond air mill for the preparation of spherical single-crystals. Amer. Mineral., 73(5-6): 662-666.

Pankow, K.L., Williams, Q. and Lay, T., 2002. Using shear wave amplitude patterns to detect metastable olivine in subducted slabs. J. Geophys. Res. - Solid Earth, 107(B6): 16.

Paterson, M.S., 1982. The determination of hydroxyl by infraredabsorption in quartz, silicate glasses and similar materials, 105: 20-19.

Peacock, S.M., 2001. Are the lower planes of double seismic zones caused by serpentine dehydration in subducting oceanic mantle? Geology, 29(4): 299-302.

Ranero, C.R., Morgan, J.P., McIntosh, K. and Reichert, C., 2003. Bending-related faulting and mantle serpentinization at the Middle America trench. Nature, 425(6956): 367-373.

Rubie, D.C., 1986. The catalysis of mineral reactions by water and restrictions on the presence of aqueous fluid during metamorphism. Mineral. Mag., 50, 399-415.

Rubie, D.C., 1996. Phase transformations in the Earth's mantle. In Mellini, M., Ranalli, G., Ricci, C.A., Trommsdorff, V. (Eds.), High Pressure and Temperature Research on Lithosphere and Mantle Minerals Proceedings of the International School of Earth and Planetary Sciences, Sienna, 41-66.

Rubie, D.C. and Ross, C.R., 1994. Kinetics of the olivine-spinel transformation in subducting lithosphere - experimental constraints and implications for deep slab processes. Phys. Earth Planet. Inter., 86(1-3): 223-241.

Rubie, D.C., Tsuchida, Y., Yagi, T., Utsumi, W., Kikegawa, T. Shimomura, O. and Brearly, A.J., 1990. An in situ x-ray-diffraction study of the kinetics of the $Ni_2SiO_4$ olivine-spinel transformation. J. Geophys. Res. - Solid Earth Planets, 95(B10): 15829-15844.

Smyth, J.R., Miyajima, N., Huss G.R., Hellebrand, E., Rubie, D.C., Frost, D.J., 2012. Olivine‐wadsleyite‐pyroxene topotaxy: Evidence for coherent nucleation and diffusion-controlled growth at the 410-km discontinuity. Phys. Earth Planet. Inter. 200-201: 85-91.

Sung, C.M. and Burns, R.G., 1976a. Kinetics of high-pressure phase-transformations - implications to evolution of olivine-spinel transition in downgoing lithosphere and its consequences on dynamics of the mantle. Tectonophysics, 31(1-2): 1-32.

Sung, C.M. and Burns, R.G., 1976b. Kinetics of olivine-] spinel transition - implications to deep-focus earthquake genesis. Earth Planet. Sci. Lett., 32(2): 165-170.

Tenner, T.J., Hirschmann, M.M., Withers, A.C. and Hervig, R.L., 2009. Hydrogen partitioning between nominally anhydrous upper mantle minerals and melt between 3 and 5 GPa and applications to hydrous peridotite partial melting. Chem. Geol., 262(1-2): 42-56.

Tetzlaff, M. and Schmeling, H., 2000. The influence of olivine metastability on deep subduction of oceanic lithosphere. Phys. Earth Planet. Inter., 120(1-2): 29-38.

Tetzlaff, M. and Schmeling, H., 2009. Time-dependent interaction between subduction dynamics and phase transition kinetics. Geophysical Journal International, 178(2): 826-844.

Turnbull, D. 1956. Phase changes. Solid State Physics, 3, 225-306.

van der Hilst, R., Engdahl, R., Spakman, W. and Nolet, G., 1991. Tomographic imaging of subducted lithosphere below northwest pacific island arcs. Nature, 353(6339): 37-43.

Wiens, D.A., McGuire, J.J. and Shore, P.J., 1993. Evidence for transformational faulting from a deep double seismic zone in Tonga. Nature, 364(6440): 790-793.

Withers, A. C., Hirschmann, M. M., and Tenner, T. J., 2011. The effect of Fe on olivine $H_2O$ storage capacity: Consequences for $H_2O$ in the martian mantle. Amer. Mineral., 96(7): 1039-1053.

Yoshioka, S., Daessler, R., and Yuen, D.A., 1997. Stress fields associated with metastable phase transitions in descending slabs and deep-focus earthquakes. Phys. Earth Planet. Inter., 104: 345-361.

Young, T. E., H. W. Green, A. M. Hofmeister, and D. Walker, 1993. Infrared spectroscopic investigation of hydroxyl in beta-$(Mg,Fe)_2SiO_4$ and coexisting olivine - Implications for mantle evolution and dynamics. Phys. Chem. Miner., 19(6): 409-422.

Zhao, Y.H., Ginsberg, S.B. and Kohstedt, D.L., 2004. Solubility of hydrogen in olivine: dependence on temperature and iron content. Contrib. Mineral. Petrol., 147(2): 155-161.

Table 1
Summary of $H_2O$ measured in olivine experimentally hydrated at 2 GPa, 950 °C, for 48 hrs.

| PC RUN | Samples Measured | $H_2O$ (ppmw) |
|---|---|---|
| PC6 | 2 | 60(8)† |
| PC8 | 1 | 46(8)† |
| PC10 | 2 | 72(20)† |
| PC11 | 1 | 52(18)† |
| PC20 | 1 | 67(7)‡ |
| PC22 | 1 | 61(9)‡ |
| | 1 | 88(9)* |
| PC31 | 1 | 75(10) ‡ |

† Measured on Cameca 6f w/ standards separate. Error estimates for H2O contents provided in parentheses.
‡ Measured on Cameca 7f w/ standards present on the same mount. Error estimates for H2O contents provided in parentheses.
* Measured with FTIR using Bell et al. (2003) calibration. Errors in H2O provided in parentheses estimated from uncertainty in the baseline.

Table 2
Transformation experiments of nominally anhydrous olivine at 18 GPa.

| MA RUN | T (°C) | t (hrs) | Rim thickness (μm) | $H_2O$ core (ppmw) | $H_2O$ rim estimate (ppmw) | Bulk $H_2O$ estimate[¥] (ppmw) |
|---|---|---|---|---|---|---|
| **Method 1 runs.** | | | | | | |
| BB611 | 1000 | 0.50 | 8(6) | 8(1)‡ | | 10 |
| | | | | 15(3)* | | |
| BB609 | 1000 | 1.00 | 34(9) | 24(19)* | ≥100** | 40 |
| BB616 | 1000 | 1.00 | 64(22) | 24(10)‡ | ≤800‡ | 40 |
| BB622 | 1000 | 1.00 | 26(6) | 13(1)‡ | ≤20‡ | 20 |
| | | | | 17(12)* | | |
| BB621 | 1100 | 1.13 | 32(13) | | | |
| BB603 | 1000 | 2.00 | 55(36) | | ≤2000† | |
| BB623 | 1000 | 2.00 | 8(5) | | | |
| BB625 | 1000 | 3.00 | 29(12) | | | |
| BB606 | 1000 | 6.00 | 23(21) | | | |
| **Method 2 runs.** | | | | | | |
| BB675 | 1000 | 0.17 | 3(2) | 7(2)‡ | | 5 |
| | | | | 2(2)* | | |
| BB660 | 1000 | 0.43 | 7(1) | <5‡ | | <6 |
| BB656 | 1000 | 1.00 | 11(3) | <5‡ | | <6 |
| BB653 | 1000 | 6.00 | 12(2) | 6(3)‡ | | 6 |
| BB688 | 1000 | 30.00 | 38(7) | 19(3)‡ | ≤300‡ | 30 |
| | | | | 17(3)* | ≥200** | |

† Measured on Cameca 6f w/ standards separate.
‡ Measured on Cameca 7f w/ standards present. Errors estimates for $H_2O$ contents provided in parentheses
* Measured with FTIR using Bell et al. (2003) calibration. Errors in $H_2O$ provided in parentheses calculated from uncertainty in baseline. Larger rim and bulk $H_2O$ content errors estimated based on rim geometry.
** Estimated minimum rim $H_2O$ content using unpolarized IR with Paterson (1982) calibration.
[¥] Bulk $H_2O$ contents estimated from $H_2O$ in the core, rim thickness, and 3.4 $Rw(H_2O)/Ol(H_2O)$ ratio from Diedrich et al. (2009).

Table 3
Transformation of experimentally hydrated olivine at 18 GPa.

| MA RUN | Sample | Exp. method | T (°C) | t (hrs) | Rim thickness (μm) | $H_2O$ core (ppmw) | $H_2O$ rim estimate (ppmw) | Bulk $H_2O$ estimate[¥] (ppmw) |
|---|---|---|---|---|---|---|---|---|
| BB519B | PC9 | 1 | 700 | 24.00 | 5(2) | | | |
| BB536A | PC11 | 1 | 700 | 72.00 | 14(3) | | | |
| BB684B | PC22 | 2 | 700 | 48.00 | 9(3) | | | |
| BB764 | PC31 | 2 | 700 | 95.00 | 10(3) | | | |
| BB522A | PC9 | 1 | 900 | 1.00 | 16(12) | | | |
| BB522B | PC9 | 1 | 900 | 1.00 | 15(10) | | | |
| BB553 | PC11 | 1 | 900 | 2.50 | 34(26) | 100(30)† | | 150 |
| BB533A | PC11 | 1 | 900 | 4.00 | 44(5) | | | |
| BB533B | PC11 | 1 | 900 | 4.00 | 43(4) | | | |
| BB521B | PC9 | 1 | 900 | 7.00 | 62(11) | | | |
| BB554 | PC11 | 1 | 900 | 10.00 | 74(21) | 20(20)‡ | ≤400‡<br>≤300† | 40 |
| BB680 | PC22 | 2 | 900 | 1.05 | 16(6) | 74(7)* | | 90 |
| BB755 | PC31 | 2 | 900 | 7.00 | 31(23) | | | |
| BB754A | PC31 | 2 | 900 | 26.13 | 115(57) | | | |
| BB754B | PC31 | 2 | 900 | 26.13 | 109(54) | | | |
| BB550 | PC11 | 1 | 1100 | 0.08 | 41(9) | 42(6)† | | 70 |
| BB527A | PC11 | 1 | 1100 | 0.17 | 52(8) | | | |
| BB583 | PC10 | 1 | 1100 | 0.25 | 56(7) | | | |
| BB588 | PC10 | 1 | 1100 | 0.33 | 74(14) | 72(25)† | ≤300† | 140 |
| BB770 | PC31 | 2 | 1100 | 0.03 | 6(1) | | | |
| BB678 | PC22 | 2 | 1100 | 0.33 | 69(21) | | | |
| BB759A | PC31 | 2 | 1100 | 0.67 | 53(19) | | | |
| BB759B | PC31 | 2 | 1100 | 0.67 | 41(11) | | | |

† Measured on Cameca 6f w/ standards separate. Error estimates for $H_2O$ contents provided in parentheses
‡ Measured on Cameca 7f w/ standards present. Error estimates for $H_2O$ contents provided in parentheses
* Measured with FTIR using Bell et al. (2003) calibration. Errors in $H_2O$ provided in parentheses calculated from uncertainty in baseline. Larger rim and bulk $H_2O$ content errors estimated based on rim geometry.
[¥] Bulk $H_2O$ contents estimated from $H_2O$ in the core, rim thickness, and 3.4 $Rw(H_2O)/Ol(H_2O)$ ratio from Diedrich et al. (2009).

Table 4.
Growth rate fitting results.

| **Fitting Equation** | **$\dot{x}$ (m/s) 700 °C** | **$\dot{x}$ (m/s) 900 °C** | **$\dot{x}$ (m/s) 1100 °C** | **ΔH (kJ/mol)** |
|---|---|---|---|---|
| mx+b (uw) | 2.5(1.6)E-11 | 1.0(0.1)E-09 | 8.9(3.0)E-08 | 226(37) |
| mx (uw) | 4.1(0.7)E-11 | 1.3(0.1)E-09 | 9.5(1.5)E-08 | 214(36) |
| mx+b (w) | 2.9(1.4)E-11 | 1.4(0.2)E-09 | 1.0(0.3)E-07 | 227(32) |
| mx (w) | 4.3(0.7)E-11 | 2.3(0.3)E-09 | 7.3(1.8)E-08 | 207(14) |
| mx, method 2 (uw) | 3.4E-11* | 1.2(0.1)E-09 | 5.4E-08* | 205(26) |
| mx, method 1 (uw) | 5.5E-11* | 2.4(0.2)E-09 | 9.6E-08* | 209(21) |

* Some errors n/a because < 3 points were used in fit.
uw denotes unweighted fit, w denotes weighted fit.
ΔH calculated assuming that $\Delta V_a = 0$.

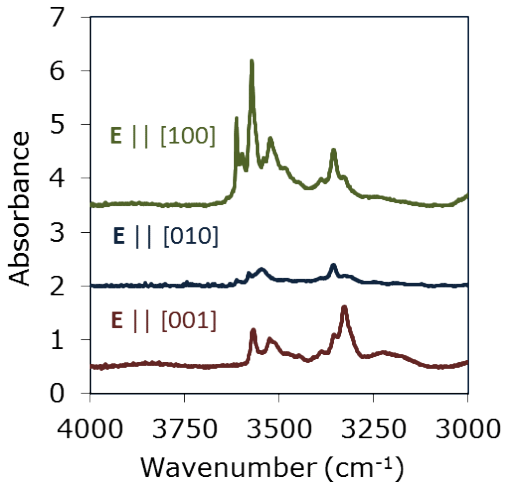


Fig. 1. FTIR absorbance in the O-H vibrational region of a hydrated olivine sphere from PC22 using transmitted light polarized parallel to each principal orientation. Spectra have been arbitrarily offset and normalized to 1 cm.

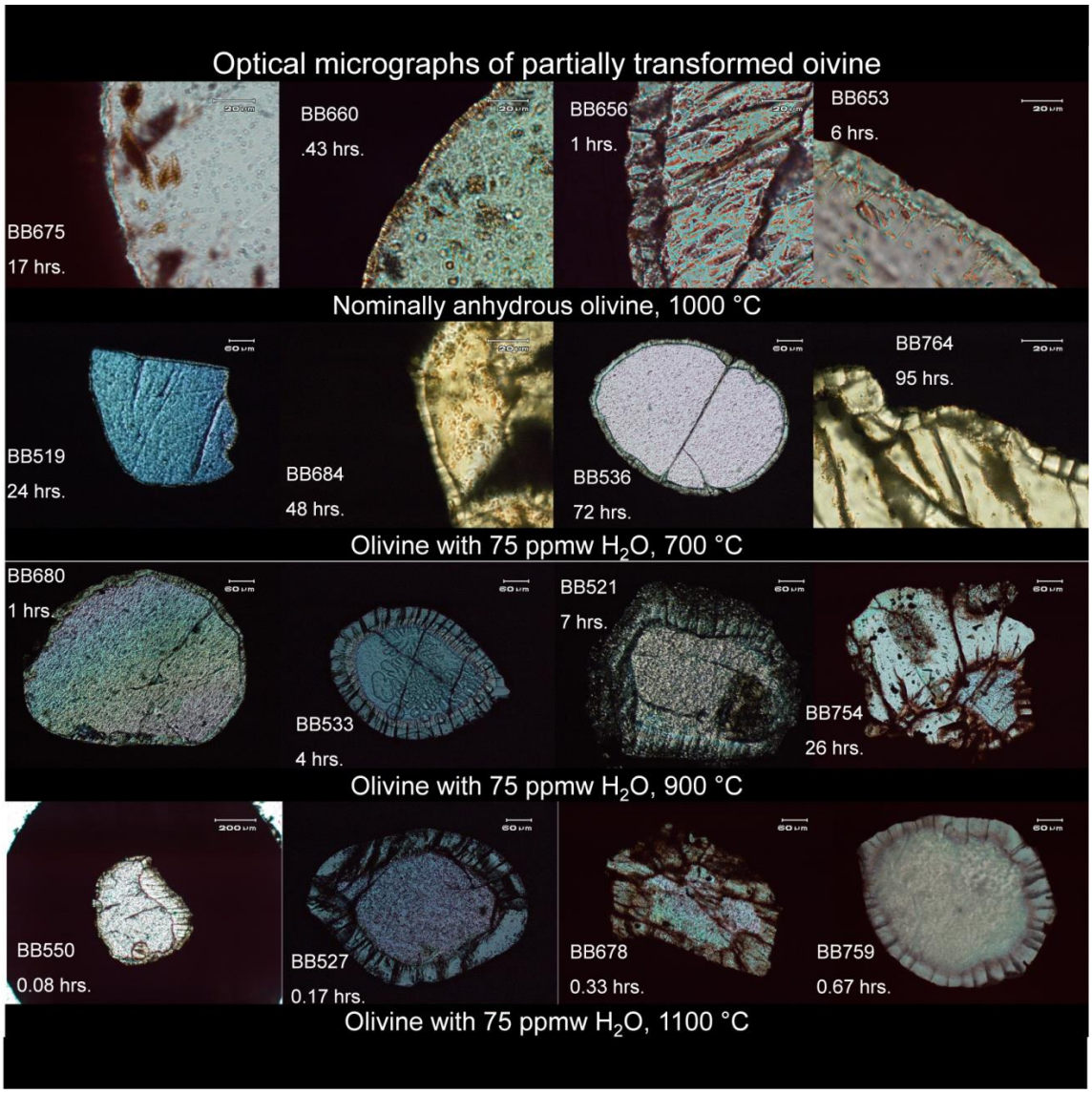
Optical micrographs of partially transformed oivine
BB675
17 hrs.
BB660
.43 hrs.
BB656
1 hrs.
BB653
6 hrs.
Nominally anhydrous olivine, 1000 °C
BB519
24 hrs.
BB684
48 hrs.
BB536
72 hrs.
BB764
95 hrs.
Olivine with 75 ppmw H2O, 700 °C
BB680
1 hrs.
BB533
4 hrs.
BB521
7 hrs.
BB754
26 hrs.
Olivine with 75 ppmw H2O, 900 °C
BB550
0.08 hrs.
BB527
0.17 hrs.
BB678
0.33 hrs.
BB759
0.67 hrs.
Olivine with 75 ppmw H2O, 1100 °C

Fig. 2. Optical micrographs of sample thin sections in plane-polarized light. Samples have growth rims surrounding an olivine core. The growth rims of nominally anhydrous olivine are relatively thin and uniform compared to those of hydrous olivine. Growth rims from hydrous olivine have variable thickness which may indicate that they are deformed.

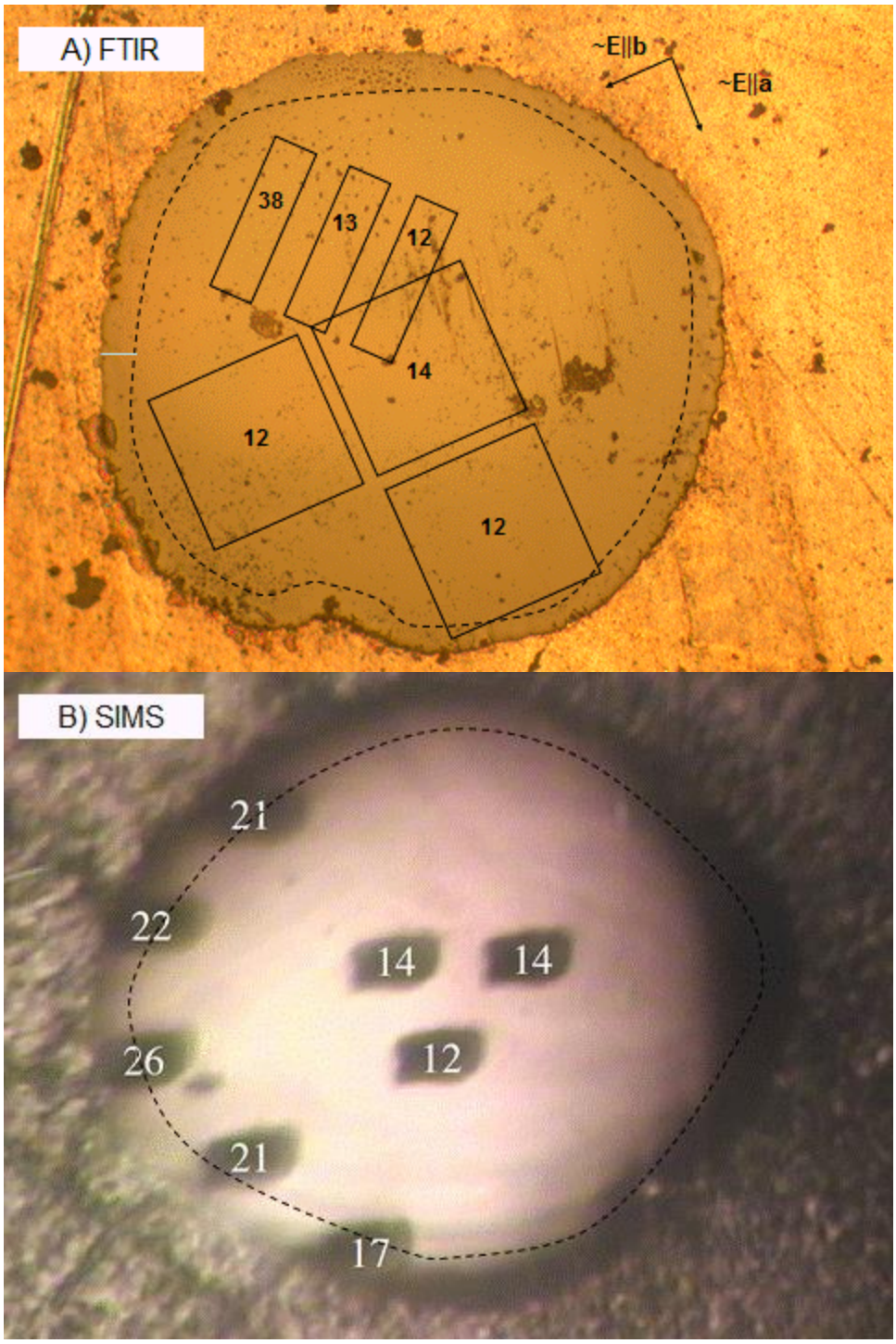
A) FTIR
~E||b
~E||a
38
13
12
14
12
12
B) SIMS
21
22
14
14
26
12
21
17

Fig. 3. Maps of $H_2O$ contents measured in sample BB622, which was partially transformed using method 1 at 18 GPa, 1000 °C, for 1 hour. Dashed lines show the approximate boundary between the outer growth rim and inner olivine core, based on rim thickness measurement of the other sphere from the same run. A.) Boxes show each area analyzed by FTIR (with ~ **E** || [100]), with estimates of $H_2O$ content displayed in ppmw. B.) SIMS analyses obtained with the Cameca 7f with $H_2O$ contents displayed in ppmw above each analysis crater.

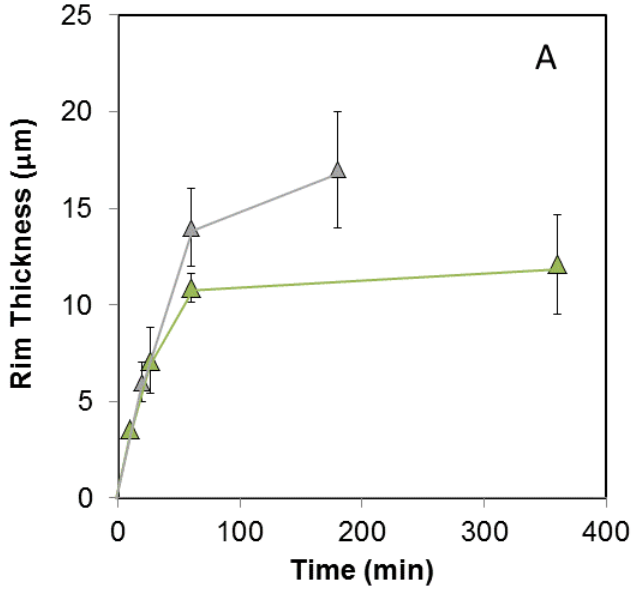
A
Rim Thickness (µm)
25
20
15
10
5
0
0
100
200
300
400
Time (min)

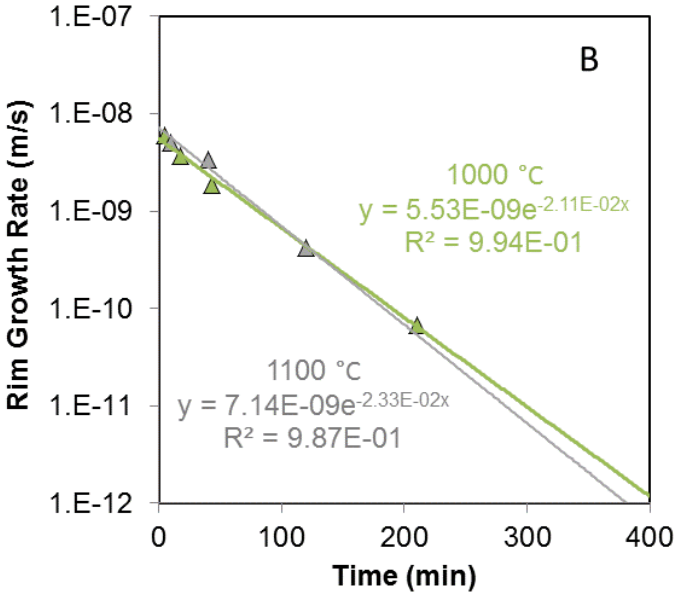
B
Rim Growth Rate (m/s)
1.E-07
1.E-08
1.E-09
1.E-10
1.E-11
1.E-12
1000 °C
y = 5.53E-09e-2.11E-02x
R² = 9.94E-01
1100 °C
y = 7.14E-09e-2.33E-02x
R² = 9.87E-01
0
100
200
300
400
Time (min)

Fig. 4. A) Growth rim thickness versus time for transformation experiments (method 2) on nominally anhydrous olivine at 1000 °C and 18 GPa. Estimates of final bulk $H_2O$ content are provided in ppmw above corresponding data points. A, B) Average growth rates (calculated using equation 1) between each experiment (green lines) versus time decreased from $5.9x10^{-9}$ to $6.8x10^{-11}$.

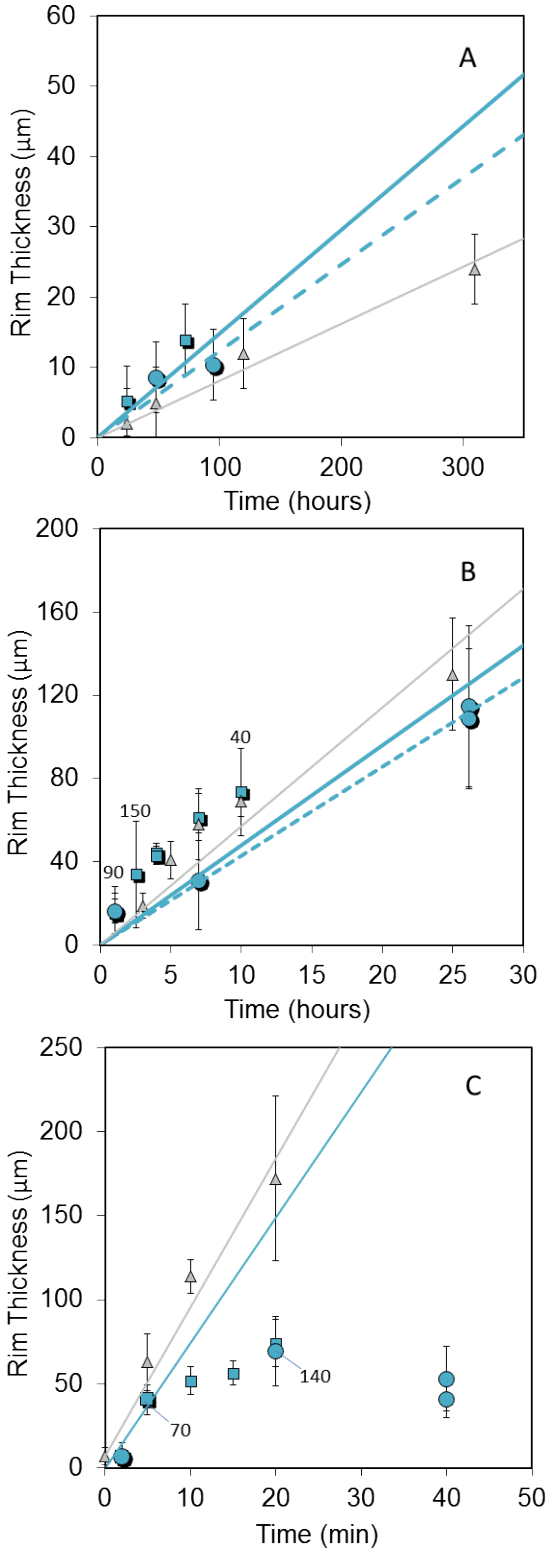
A
Rim Thickness (µm)
Time (hours)
B
Rim Thickness (µm)
Time (hours)
40
150
90
C
Rim Thickness (µm)
Time (min)
140
70

Fig. 5. Rim thickness as a function of time for olivine with 75 ppmw of $H_2O$ at 18 GPa at 700 °C (A), 900 °C (B), and 1100 °C (C). Blue squares and circles represent our ~ 75 ppmw experiments using method 1 and method 2, respectively. Estimates of final bulk $H_2O$ content are provided in ppmw next to corresponding data points. Solid blue lines are linear fits of both method 1 and 2 data, and dashed lines are linear fits of only method 2 data (dashed) with slopes equal to growth rates. At 1100 °C, data with time $\geq$ 10 minutes were excluded from the fit. For comparison, data for olivine with 300 ppm $D_2O$ are plotted as grey triangles with corresponding linear fits of this data shown as grey lines (Diedrich et al., 2009).

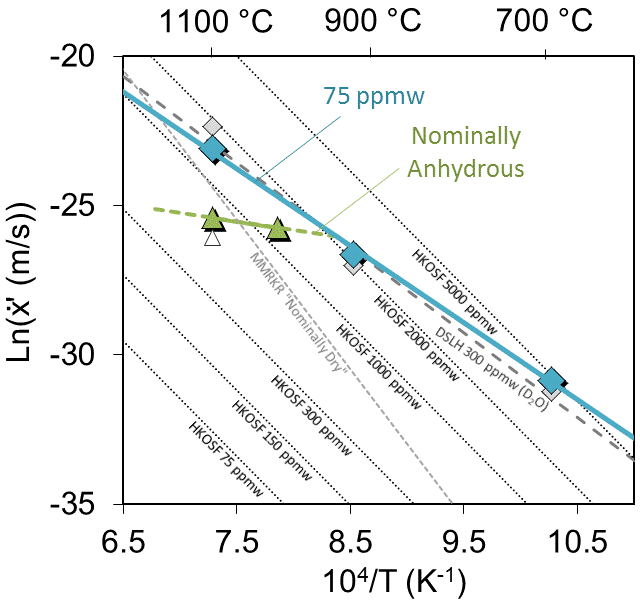


Fig. 6. Normalized growth rate, where $\dot{x}' = \dot{x}/[T(1-\exp(-\Delta G_{rxn}/RT)]$ as a function of reciprocal temperature on an Arrhenius plot. Growth rates for t = 0 shown for nominally anhydrous olivine fit using our newly proposed method - green triangles and solid green line (this study) ; and those fit using the previous method - open triangle (Diedrich et al., 2009) - solid grey line (Mosenfelder et al., 2001). Growth rates shown for olivine with 75 ppmw $H_2O$ – blue diamonds and solid blue line (this study), and for olivine with 300 ppmw $D_2O$ – grey diamonds and dashed grey line (Diedrich et al., 2009). Growth rates calculated from Hosoya et al. (2005) shown for olivine with various $H_2O$ contents - dotted grey lines.